Simultaneous determination of grain and grain-boundary critical currents in $YBa_2Cu_3O_7$-coated conductors by magnetic measurements

A. Palau,* T. Puig, and X. Obradors
Institut de Ciència de Materials de Barcelona, CSIC, Campus de la UAB, 08193 Bellaterra, Spain

Ch. Jooss
Institut für Materialphysik, University of Göttingen, D-37075 Göttingen, Germany

(Received 26 July 2006; revised manuscript received 5 December 2006; published 21 February 2007)

We present a complete description of a noninvasive inductive methodology developed to study the magnetic granularity inherent in coated conductors. The method is based on the analysis of coated conductor hysteresis loops and enables us to identify the presence of electromagnetic granularity from the appearance of a peak in the return branch of the irreversible magnetization. Minor hysteresis loop cycles reveal the evolution of this peak and allow us to separate and analyze independently grain, grain-boundary critical current densities, and grain size of coated conductors. We have performed different tests to the developed model in order to validate the main assumptions considered and better understand the key factors involved.

DOI: 10.1103/PhysRevB.75.054517 PACS number(s): 74.25.Sv, 75.75.+a, 81.05.Rm

I. INTRODUCTION

$YBa_2Cu_3O_7$- (YBCO-) coated conductors are now considered as one of the most promising materials for developing high-T_c superconductor based tapes to be used in electric power applications. However, in order to achieve high critical current densities J_c exceeding 3×10^{10} A/m^2 at $T=77$ K and self field, it is necessary to texture the superconductor layer avoiding large-angle grain boundaries (GBs). Ion-beam-assisted deposition (IBAD) and Rolling-assisted biaxially textured substrate (RABiTS) techniques have shown to be suitable for the preparation of highly biaxially textured coated conductors.[1,2] However, in general, coated conductors behave like granular material, except for some recent IBAD samples having a very high orientational order.[3,4]

The influence of low-angle grain boundaries on current percolation has been a crucial issue since very early stages when the strong dependence of the transport critical current density with the grain misorientation was observed.[5,6] Since then, understanding current percolation through a network of grain boundaries has been handled by several authors[6–9] and many works have been reported trying to simulate the probability of percolation through a sample and the restricting paths for current flow.[10–13]

Presently, a granular coated conductor is considered as a superconducting network of low-angle grain boundaries through which a percolative current flows separating superconducting grains. Two mechanisms are basically involved in the current transport of these systems: the dissipation mechanisms associated to the grain-boundary network J_c^{GB} and the vortex physics associated to the grain critical current density J_c^G. Whereas Abrikosov vortices are clearly governing the vortex pinning properties of the grains, the physical mechanisms associated to the dissipation of the grain-boundary network are somewhat more complicated. Dissipation associated to Abrikosov-Josephson vortices at the grain boundaries,[14] their properties and interaction with the Abrikosov vortices is one of the most interesting topics nowadays.[15–18]

Previous studies have been developed in order to determine the magnetic grain size[19] and the grain and grain-boundary critical current densities[20,21] by means of inductive measurements. However, in general, they cannot be used when the values of J_c^G and J_c^{GB} are differentiated in less than a factor 2–5. Additionally, complex nano-patterning techniques,[22] have been applied in order to measure the critical current density of one grain and one grain boundary. This complex procedure though, cannot be reproduced in a systematic manner since it's very cumbersome. In this contribution we present a complete analysis of a noninvasive inductive methodology based on dc magnetometry, briefly described in, Ref. 23, which is able to determine simultaneously J_c^G and J_c^{GB} of high quality coated conductors with $J_c^{GB}\sim J_c^G$ without the requirement of any patterning on the samples. Hence, this method can be used to systematically study the relationship between J_c^G and J_c^{GB} in different situations of great interest such us the effect of the strain induced in the tapes,[24] the thickness of YBCO layer[25] or the correlation of the YBCO grains with the substrate grains.[26] We present a fully consistent analysis of magnetization loops in coated conductors which represent a strong advancement in detailed understanding of granular systems and facilitates the study of relevant problems which can only be addressed by knowing the relationship between J_c^G and J_c^{GB}. In this paper we describe the peculiarities and assumptions considered in the developed methodology and we check their consistency. The layout of the paper is as follows. Section II contains the experimental details. In Sec. III we present a complete analysis of the feature of magnetic hysteresis loops measured for YBCO-coated conductors. Section IV describes the theoretical methodology developed to determine J_c^{GB}, J_c^G and the average magnetic grain size $\langle 2a\rangle$ for a given coated conductor. In Sec. V we show several tests performed to the model which demonstrate its steadiness and verify the validity of the assumptions considered. Conclusions are shown in Sec. VI.

II. EXPERIMENTAL DETAILS

Several high-quality YBCO-coated conductors grown by pulsed laser deposition[27] (PLD) on CeO_2/IBAD-YSZ/Ni-Cr stainless steel substrates and by a BaF_2 *ex situ* process using evaporated precursors on CeO_2/YSZ/Y_2O_3/Ni/Ni-3%W RABiTS tapes[28] were analyzed. All the samples were cut into small pieces of about 5 mm×5 mm and an effective sample radius R was determined by considering a disk with a surface equal to the sample surface S, i.e., $S=\pi R^2$.

Magnetic measurements were conducted with a superconducting quantum interference device magnetometer provided with a 5.5 T superconducting coil which allowed a temperature variation in the sample space from 5 K to room temperature. Samples were mounted with the dc magnetic field applied perpendicular to the substrate and standard measurements of magnetic hysteresis loops were measured cooling the sample in zero field (ZFC). Transport measurements were performed in a 9 T cryostat with temperature variable from 5 K to room temperature. Critical current densities were determined by using a 1 μV/cm criteria. The magnetic field was also applied perpendicular to the substrate. Magnetic field imaging was done by measuring the magnetic-flux density distribution by a magneto-optical (MO) technique[29] after applying an external field perpendicular to the sample substrate.

III. MAGNETIC HYSTERESIS LOOPS

Before analyzing the magnetic hysteresis loops measured for YBCO-coated conductors, subtraction of the magnetic-substrate contribution to the total magnetic moment was required. This contribution was especially important for RABiTS-coated conductors due to the large magnetic signal coming from the nickel substrate. For IBAD samples with low-magnetic stainless steel tapes, the magnetic moment coming from the substrate could be directly removed by subtracting the hysteresis loop measured for a piece of substrate. In this process it was important to use a substrate with the same geometrical shape as the coated conductor, in order to minimize demagnetizing effects sensitive to the sample geometry. Moreover, we had to measure the coated conductor and the substrate loops at the same temperature since the dependence of the stainless steel magnetic moment with temperature in the working range (5–77 K) was significant. In contrast, for RABiTS-coated conductors, the temperature dependence of the nickel magnetic moment was constant at the range of temperatures considered (5–100 K). In that case, we could directly obtain the signal coming from the substrate by measuring the coated conductor at a temperature higher than the YBCO critical temperature (100 K) where the superconducting layer did not give any signal. The superconductor signal was then obtained by subtracting a hysteresis loop measured at 100 K to the one measured at the desired temperature. With this procedure we could directly determine the signal of the sample substrate avoiding any error induced by using slightly different substrate shapes giving rise to different demagnetizing effects, especially strong in nickel tapes. Figure 1 shows a typical coated conductor hysteresis loop measured for a RABiTS sample with thickness $t=1.08$ μm and texture $\Delta\phi=6.3°$, RABiTS-a, after substrate subtraction for a maximum applied field $\mu_0 H_m=0.5$ T at 5 K (open symbols). This has been compared with the hysteresis loop measured for a non-granular thin film, with $t=0.27$ μm and $\Delta\phi=0.6°$, film-a, at the same conditions (closed symbols), in order to analyze the effect that inherent granularity of coated conductors produce to the magnetic hysteresis loops. It should be noted that the coated conductor hysteresis loop appears to be anomalous with a maximum on the reverse branch of the magnetization at a positive applied magnetic field $\mu_0 H_a=0.24$ T, instead of at $\mu_0 H_a=0$ T as expected for a superconducting nongranular film.[30]

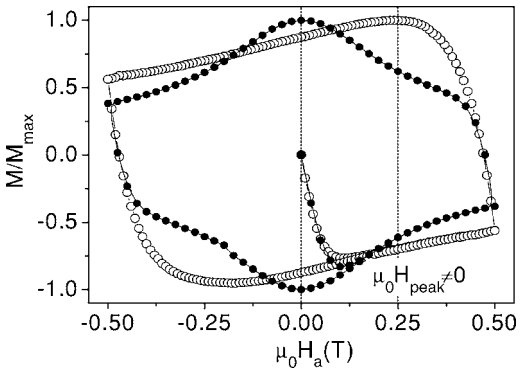

FIG. 1. Magnetic hysteresis loops measured at $T=5$ K and $\mu_0 H_m=0.5$ T, for film-a (closed symbols) and for the coated conductor RABiTS-a (open symbols).

Similar peaks were previously observed in BSCCO tapes,[31] YBCO films with artificial granularity,[32] and recently in YBCO bicrystals.[33] In these systems the effect of having a peak in the reverse magnetization at $H_a>0$, could be ascribed to granularity effects and explained by the same mechanism as that of the hysteretic behavior of J_c observed in transport measurements of polycrystalline samples.[34] The considered model describes the shift of the magnetization peak and the anomalous resulting hysteresis loops by means of the trapped field within the grains, which induce a reverse magnetic field through the grain boundaries.[23] As the applied magnetic field is ramped up, flux enters the material and gets pinned into the grains, subsequent decrease of the magnetic field results in a reverse magnetic field component at the grain edges. Thus, the local magnetic field at the grain boundaries $H_{\mathrm{loc}}{}^{\mathrm{GB}}$ results from the vectorial sum of the applied magnetic field H_a and the reverse field at the edge of each grain that goes through the grain boundary H_{edge}:

$$H_{\mathrm{loc}}^{\mathrm{GB}} = H_a - H_{\mathrm{edge}}. \tag{1}$$

The magnetization peak appears when $H_{\mathrm{loc}}{}^{\mathrm{GB}}=0$, and thus when $H_{\mathrm{peak}} \sim H_{\mathrm{edge}}$. If the magnetic field is then decreased until $H_a=0$, the local field at the grain boundaries will be given by H_{edge} at zero applied field $H_{\mathrm{loc}} \sim -H_{\mathrm{edge}}(H_a=0)$.

Figure 2 shows several magnetic hysteresis loops measured for RABiTS-a at 5 K with different values of H_m. As the maximum applied field H_m increases, the value of the magnetic field where the maximum of the magnetization appears H_{peak} increases until it saturates.

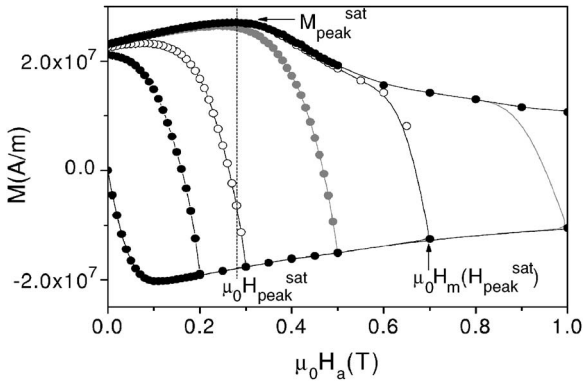

FIG. 2. Magnetic hysteresis loops at 5 K measured for the RABiTS coated conductor RABiTS-a with $\mu_0 H_m$=0.2, 0.3, 0.5, 0.7, 1, and 2 T.

Figure 3 shows the evolution of H_{peak} as a function of H_m determined from the hysteresis loops presented in Fig 2. Clearly, H_{peak} increases for low values of H_m and then it saturates in reproducing the evolution of the trapped field in the grains. So that, from these measurements we can determine the maximum applied field needed to saturate the peak position $\mu_0 H_m(H_{\text{peak}}{}^{\text{sat}}) \sim 0.7$ T, and the saturated value of H_{peak} $\mu_0 H_{\text{peak}}{}^{\text{sat}}$=0.28 T. These two magnitudes are characteristic of each coated conductor and as we will see below they will be used to determine the grain critical current density $J_c{}^G$ and average magnetic grain size $\langle 2a \rangle$.

Furthermore, we will determine the percolating GB critical current density $J_c{}^{\text{GB}}$ by means of the magnetic moment measured for a saturated hysteresis loop. We will see that the magnetic moment associated to the grain current loops is negligible compared with the magnetic moment associated to the large percolative current loops described by the GB currents. Hence, the total magnetic moment measured in the hysteresis loop correspond only to the contribution of the GBs and thus, the saturated value of the magnetization at the peak position $M_{\text{peak}}{}^{\text{sat}}$=27 MA/m, will be used to find the GB critical current density at $\mu_0 H_{\text{loc}}$=0 T.

The same shift in the magnetization peak has also been observed in IBAD samples, confirming that granularity effects can be detected in both types of coated conductors. The

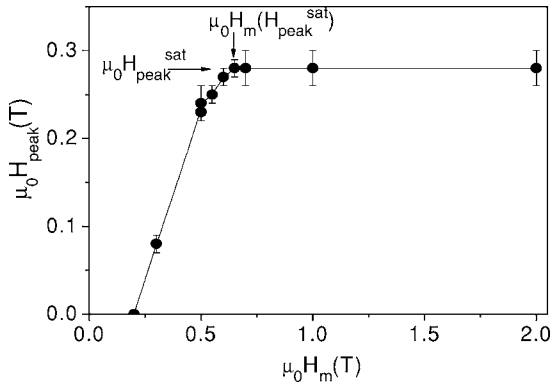

FIG. 3. Evolution of the peak position H_{peak} with the maximum applied field H_m for RABiTS-a at 5 K. We have indicated with arrows the saturated values $H_{\text{peak}}{}^{\text{sat}}$ and $H_m(H_{\text{peak}}{}^{\text{sat}})$.

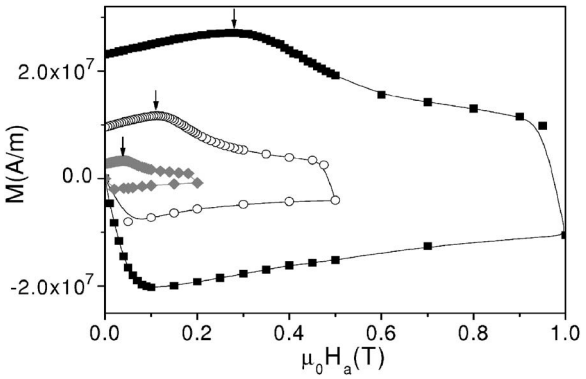

FIG. 4. Saturated hysteresis loops obtained for the sample RABiTS-a at T=5 K (■), 50 K (○), and 77 K (◆) for $\mu_0 H_m$=1, 0.5, and 0.2 T, respectively. Arrows show the magnetic field at the peak.

comprehension of the phenomenon that induces the peculiar anomalous coated conductor hysteresis loops, i.e., a peak in the reverse magnetization at $H_a > 0$, has allowed us to develope a unique methodology able to determine both $J_c{}^G$ and $J_c{}^{\text{GB}}$ independently.

Figure 4 shows three saturated hysteresis loops measured at different temperatures for RABiTS-a. It should be noted that both the value of $M_{\text{peak}}{}^{\text{sat}}$ and $H_{\text{peak}}{}^{\text{sat}}$ decrease by increasing temperature. We will see that $J_c{}^{\text{GB}}$ and $J_c{}^G$ are proportional to $M_{\text{peak}}{}^{\text{sat}}$ and $H_{\text{peak}}{}^{\text{sat}}$, respectively, and thus a decrease of these values with temperature is associated with a decrease of $J_c{}^{\text{GB}}(T)$ and $J_c{}^G(T)$. The evolution of H_{peak} with the maximum applied field H_m measured at different temperatures is shown in Fig. 5. The maximum field that saturates the peak position $H_m(H_{\text{peak}}{}^{\text{sat}})$, also decrease by increasing temperature since, as we will see below, it will be related to the full penetration field of the grains H^*_G, which also depends on $J_c{}^G(T)$.

IV. CRITICAL CURRENT DENSITIES DETERMINATION $J_C{}^G$ AND $J_C{}^{\text{GB}}$

The model used in this analysis considers that the anomalous peak observed in the magnetic hysteresis loop of YBCO-coated conductors can be explained by means of the

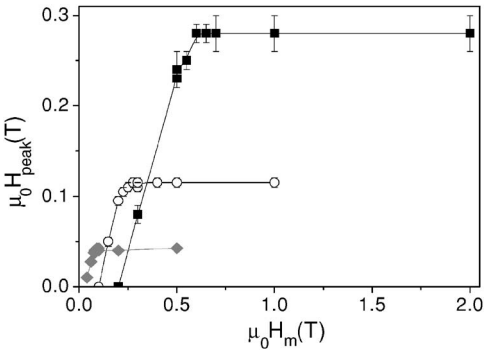

FIG. 5. $\mu_0 H_{\text{peak}}$ as a function of $\mu_0 H_m$ obtained for RABiTS-a at T=5 K (■), 50 K (○), and 77 K (◆).

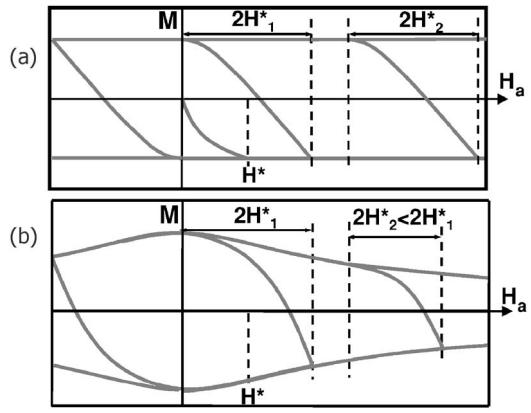

FIG. 6. Hysteresis loops calculated for a thin disk considering the Bean critical state model (a) and measured for a real thin film with $J_c(H)$ (b) at different maximum applied fields.

magnetic flux trapped inside the grains which have a reverse magnetic field component through the grain boundaries. Therefore, the local magnetic field at the grain boundaries can be determined by Eq. (1). In fact, we would have to consider the contribution of the self-magnetic field arising from the percolating GB critical current density H_{self}^{GB}, i.e., $H_{loc}^{GB}=H_a+H_{self}^{GB}-H_{edge}$. However, critical state model calculations[35,36] evidenced that this field can be neglected in the reverse magnetization curve for thin films and thus the local magnetic field has been considered to be uniform over the sample.

The condition $H_{loc}^{GB}=0$ at the peak position, i.e., $H_{peak} \sim H_{edge}$, establishes that the saturated value of the magnetic field at the peak position H_{peak}^{sat} is reached when the grain magnetization saturates and thus,

$$H_{peak}^{sat}(T) = H_{edge}^{max}(T). \tag{2}$$

Moreover, the maximum applied field needed to saturate $H_{peak} \sim H_{edge}$, $H_m(H_{peak}^{sat})$ is a measure of the magnetic field required to saturate the grain magnetization at the peak position and thus

$$H_m(H_{peak}^{sat}) - H_{peak}^{sat} = 2H_G^*, \tag{3}$$

where H^*_G is the full penetration field of the grains. However the determination of H^*_G by means of the grain magnetization saturation at $H_a=H_{peak}^{sat}$ will give us an underestimated value in comparison with the one we would obtain at $H_a=0$, due to the field dependence of $J_c^G(H)$. This is illustrated in Fig. 6.

Figure 6(a) shows several hysteresis loops calculated for a cylindrical thin film according to the Bean critical state model, i.e., J_c independent of the magnetic field, for different maximum applied fields.[30] The equivalent loops measured for a real thin film with a certain $J_c(H)$ dependence are shown in Fig. 6(b). In the calculations considering the Bean critical state model, saturation of the magnetization at $H_a=0$ (position 1) requires the same value of $2H^*$ than saturation at $H_a>0$ (position 2), i.e., $2H^*_1=2H^*_2$. However, if a $J_c(H)$ dependence is considered [Fig. 6(b)], saturation at $H_a=0$ requires a higher applied magnetic field than saturation at $H_a>0$, i.e., $2H^*_1>2H^*_2$.

Therefore, in order to find the value of $2H^*_G$ at $H_a=0$, i.e., the saturation of the grain magnetization at $H_a=0$, one has to consider the saturation of $H_{edge}(H_a=0)$. This has been done by measuring the saturation of the remanent magnetization at $H_a=0$, $H_m(M_{rem}^{sat})$. Considering the relation $H_{loc} \sim -H_{edge}(H_a=0)$ shown above, the maximum applied field that saturates the remanent magnetization $H_m(M_{rem}^{sat})$, corresponds to the applied magnetic field that saturates the local magnetic field at the GBs at $H_a=0$, i.e., that saturates the reverse magnetic field $H_{edge}(H_a=0)$, and therefore $H_m(M_{rem}^{sat}) \sim 2H^*_G$. However, in this process, we have to ensure that the saturation of the remanent magnetization is due to the saturation of $H_{edge}(H_a=0)$ (saturation of the grain magnetization) and not owing to the saturation of the GB magnetization. Consequently, we have to verify that the full penetration field associated to the grains is higher than that associated to the whole sample, $H^*_G>H^*_S$. This condition occurred for all the samples analyzed. Therefore, Eq. (4) will be used instead of Eq. (3) to determine the full penetration field of the grains

$$H_m(M_{rem}^{sat}) = 2H_G^* \text{ for } H_G^* > H_S^*. \tag{4}$$

Then, the saturated value of the reverse field coming from the grains H_{edge}^{max} can be determined by measuring the saturated applied magnetic field at the magnetization peak $H_{edge}^{max} \sim H_{peak}^{sat}$ and the value of the grains full penetration field H^*_G can be calculated by means of the experimental value $H_m(M_{rem}^{sat})$ according to Eq. (4). In that case we are able to determine the grain critical current density J_c^G and the magnetic average grain size $\langle 2a \rangle$ by using the theoretical relations $J_c^G(H_{edge})$ and $J_c^G(H^*_G)$, described below, which only depend on the aspect ratio of grain radius vs thickness a/t.

The dependence $J_c^G(H_{edge})$ has been calculated for saturated cylinders of different aspect ratios a/t, in order to emulate the grains composing IBAD and RABiTS-coated conductors. We have assumed J_c independent of the magnetic field (Bean critical state model), and that two isolated adjacent grains (zero separation) contribute to the reverse component of the magnetic field at their grain boundary. According to these calculations the grain critical current density can be determined by[23]

$$J_c^G = \frac{H_{edge}^{max}}{xt} \approx \frac{H_{peak}^{sat}}{xt}, \tag{5}$$

where x is a numerically calculated dimensionless factor depending on the a/t ratio shown in Fig. 7.

Additionally, the full penetration field for cylinders of different aspect ratios a/t has been calculated by using a numerical simulation based on energy minimization, considering the Bean critical state model corrected by a geometric factor due to demagnetization effects.[23,30] Results for any value of $2a/t$ can be expressed as

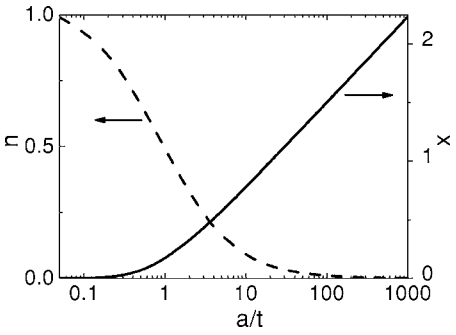

FIG. 7. Numerically calculated dimensionless factors n and x, as function of the ratio a/t.

$$H^* = J_c n a, \tag{6}$$

where n is a numerically calculated dimensionless factor depending on the a/t ratio shown in Fig. 7. So that, by using Eq. (6), we obtain the $J_c{}^G(H^*{}_G)$ dependence as

$$J_c^G = \frac{H^*{}_G}{na} \approx \frac{H_m(M_{\text{rem}}^{\text{sat}})}{2na} \quad \text{for } H^*{}_G > H^*{}_S, \tag{7}$$

where the condition $H^*{}_G > H^*{}_S$ occurs for all samples analyzed. Although the critical state model is a simplistic approach to describe the magnetic response of type II superconductors it adequately determines flux penetration in superconducting samples with different shapes[30,37,38] and it has been successfully used in granular samples,[31,32] YBCO bicrystals,[33] and coated conductors.[39] In the theoretical equations shown above we have considered the Bean critical state model which is a good approximation specially in determining the critical current density at very low fields. In a first approximation these equations derived for isolated cylindrical grains are not corrected for any component of the grain-boundary self-field since this field can be neglected for thin film materials,[35,36] as commented on above. Therefore, combining Eqs. (5) and (7) we obtain

$$\frac{H_{\text{peak}}^{\text{sat}}}{H_m(M_{\text{rem}}^{\text{sat}})} = \frac{x}{2n}\frac{t}{a} = g(a/t) \tag{8}$$

which can be used to estimate the average magnetic grain size $\langle 2a \rangle$ by means of the function $g(a/t)$ shown in Fig. 8 and the experimental value $H_{\text{peak}}{}^{\text{sat}}/H_m(M_{\text{rem}}{}^{\text{sat}})$. It should be noted that with these analysis we will obtain an average magnetic grain size of grains which grain boundaries are the limiting factor of the percolative critical current density. There may be other subgrains, with very small grain-boundary misorientations which do not limit J_c and thus do not define a magnetic grain.

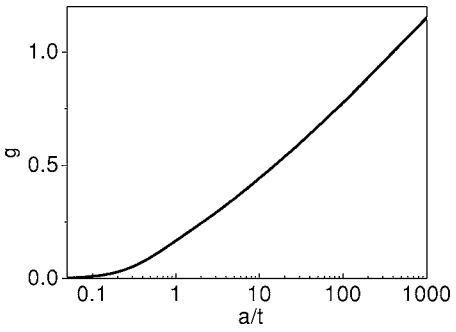

FIG. 8. Numerically calculated dimensionless factor $g(a/t)$.

We use the average magnetic grain size to calculate $J_c{}^G$ at zero applied field by means of Eq. (5) or (7), without any other free parameter. In this process we have to take into account that the reverse magnetic field component appearing in Eq. (5) $H_{\text{edge}}{}^{\text{max}}$ has not been determined at $H_a=0$ but at $H_a=H_{\text{peak}}{}^{\text{sat}}$. However, the underestimation generated in considering $H_{\text{edge}}{}^{\text{max}} \sim H_{\text{peak}}{}^{\text{sat}}$ is not significant since the magnetization peak appears close to zero and the $J_c(H)$ dependence in this region is not very important.[40]

The grain-boundary critical current density can be determined from a saturated hysteresis loop by using the following equation:[30]

$$J_c(H) = \frac{3M(H)}{R}, \tag{9}$$

where M is the magnetization at the applied magnetic field H and R the radius of the sample. In order to use that equation one has to ensure that the total magnetic moment measured in the hysteresis loop m corresponds to the magnetic moment associated to the percolative GB critical current density, i.e., $m \sim m^{\text{GB}}$. The magnetic moment associated to the grain current loops (which could include subgrains with very small grain-boundary misorinetations) m^G can be estimated by means of

$$m^G = M^G V_G N \approx \frac{J_c^G a}{3} V_G N \leqslant \frac{J_c^G a}{3} V_S, \tag{10}$$

where V_G is the grain volume, N is the number of grains, and V_S is the sample volume and a is the average magnetic grain size of grains whose grain boundaries limit the percolative J_c. Considering that the grains fill the entire sample ($N = V_S/V_G$) and $J_c{}^G = 3M^G/a$ we have obtained $m^G \sim 5 \times 10^{-2} - 10^{-3}$ m for all the coated conductors analyzed, which indicates that the large current loops described for the GB percolating currents generate a larger magnetic moment than the grain current loops associated to $J_c{}^G$. This condition would not be fulfilled if the dimension of the sample was comparable to the grain size but this is not the case in this analysis. Thus, it can be considered that the magnetic moment measured in the $m(H)$ cycles solely correspond to the magnetic moment of the GB component though strongly influenced by the reverse field component at the edge of the grains.

Figure 9 shows several $J_c{}^G$ values determined by means of Eq. (5), as a function of the average magnetic grain size $\langle 2a \rangle$ calculated with Eq. (8), for different IBAD and RABiTS conductors at 77 K. For IBAD-coated conductors we have found values of $\langle 2a \rangle$ going from 0.5 to 2.5 μm, whereas for RABiTS samples a clearly larger grain size is obtained with $\langle 2a \rangle = 20-100$ μm. These magnetic grain sizes are consistent with the structural grains determined by TEM and EBSD for the two types of coated conductors.[7,29] Note that different values of $J_c{}^G$ are reported, as we have included samples with

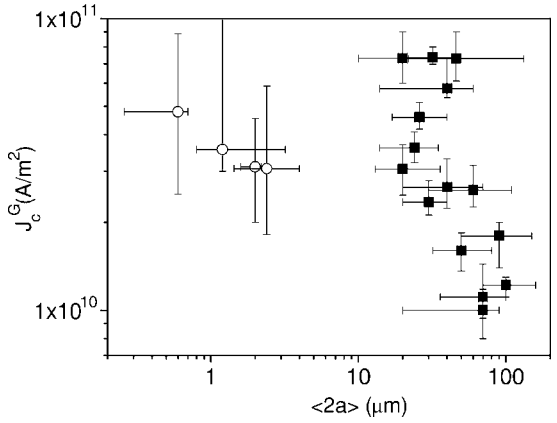

FIG. 9. Grain critical current at 77 K as a function of the average grain size determined for several IBAD (○) and RABiTS (■) coated conductors.

different thickness (from 0.2 to 2.6 μm) grown with different techniques (PLD and BaF_2). However, the large values of $J_c{}^G(77\ \mathrm{K})=1\times10^{10}\ \mathrm{A/m^2}-7\times10^{10}\ \mathrm{A/m^2}$, which are in the expected range of YBCO thin films grown on single crystals, denote that they are high quality coated conductors. It is worth noting that the same range of $J_c{}^G$ have been obtained indistinctly for both types of coated conductors, indicating that similar Abrikosov vortex pinning force can be achieved at the IBAD and RABiTS grains, although they have been grown with different techniques and they have very different grain sizes.

Figure 10 shows the J_c^{GB} values obtained using Eq. (9), for several coated conductors as a function of their full width half maximum x-ray phi scan $\Delta\phi$ at 77 K. Also included are J_c values found for two YBCO thin films grown on single crystalline substrates. The values obtained for the magnetically determined $J_c{}^{\mathrm{GB}}$ agreed well with the corresponding transport J_c (see Ref. 25). An exponential decreasing of $J_c{}^{\mathrm{GB}}(\phi)$ is observed, as it is expected,[6,9,41] though there is a certain scattering due to the different thickness, substrate or growth process of the samples analyzed. The exponential dependence indicates that grain boundaries are the most significant factor limiting $J_c{}^{\mathrm{GB}}$ values in coated conductors.

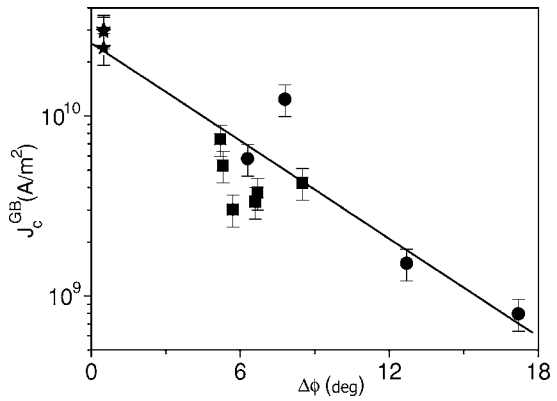

FIG. 10. $J_c{}^{\mathrm{GB}}$ as a function $\Delta\phi$ for several RABiTS (■) and IBAD (●) samples analyzed at 77 K. Also presented are some values of J_c obtained for thin films grown on single crystals (★).

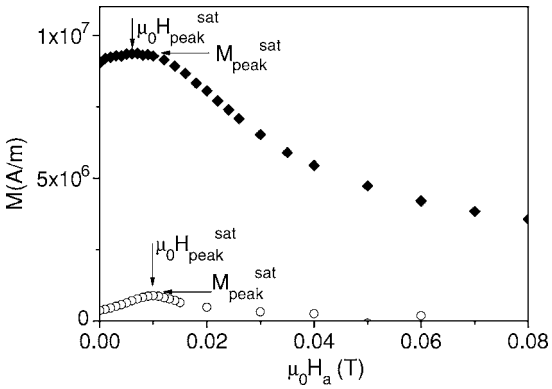

FIG. 11. Reverse branches of two saturated hysteresis loops measured at 77 K for IBAD-a (♦) and IBAD-b (○).

In order to study the texture effect in both $J_c{}^{\mathrm{GB}}$ and $J_c{}^G$, two samples with similar thickness t grown by PLD on IBAD substrates with very different texture, have been analyzed. IBAD-a with $\Delta\phi=6.5°$, $t=1$ μm and IBAD-b with $\Delta\phi=17.2°$, $t=1.6$ μm. Figure 11 shows the saturated reverse branches of hysteresis loops measured for both samples at 77 K. We observe that the two curves present a peak of magnetization at a similar position, although the magnetization is more than one order of magnitude smaller for the sample with worse texture. By determining the ratio $H_{\mathrm{peak}}{}^{\mathrm{sat}}/H_m(M_{\mathrm{peak}}{}^{\mathrm{sat}})$ and using Eq. (8), we have obtained their average magnetic grain size, being $\langle 2a\rangle=2.5$ and 3 μm for IBAD-a and IBAD-b, respectively.

By using these values of $\langle 2a\rangle$ and Eq. (5), we have determined the grain critical current density at different temperatures. Similar values of $\mu_0 H_{\mathrm{peak}}{}^{\mathrm{sat}}$ give us very similar $J_c{}^G(T)$ curves (closed symbols in Fig. 12). However, the corresponding values of $J_c{}^{\mathrm{GB}}(T)$ obtained by using Eq. (9) (open symbols in Fig. 12) are remarkably different due to the different magnetization values. For IBAD-b we have obtained $J_c{}^{\mathrm{GB}}(T)$ values about one order of magnitude lower than those found for IBAD-a. We conclude then, that the pinning of AV inside the grains does not depend on the texture of the YBCO layer since $J_c{}^G$ does not change with the sample texture whereas $J_c{}^{\mathrm{GB}}$ clearly depends on the misorientation between grains.

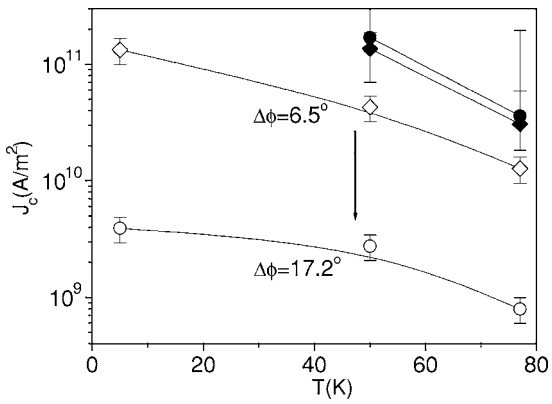

FIG. 12. Temperature dependence of $J_c{}^{\mathrm{GB}}$ (open symbols) and $J_c{}^G$ (closed symbols) for IBAD-a (diamonds) and IBAD-b (circles).

This example illustrates how the described methodology is suitable to simultaneously analyze the behavior of J_c^G and J_c^{GB} when changing different processing parameters, such us texture, substrate, growth process and it can be used to know the main factors limiting the percolative critical current density in each case. In particular, we have used this methodology to study the dependence of J_c^G and J_c^{GB} with the strain induced in IBAD and RABiTS tapes,[24] the effect of having YBCO grain-boundary networks which do not correlate with the substrate pattern[26] and the dependence of both J_c^G and J_c^{GB} with the thickness of the YBCO layer.[25] It should be noted that the present methodology enables also to determine the magnetic field dependence for J_c^{GB} though not for J_c^G, where the analysis is limited to the self-field value.

V. CONSISTENCY OF THE THEORETICAL MODEL

In this section we will evidence the strength and consistency of the magnetic methodology described above by testing it under different situations. We have also included additional measuring techniques which confirm the observed granularity effects in coated conductors.

A. Magnetic field at a grain boundary

The main idea of our model is the existence of a negative reverse magnetic field at low angle grain boundaries in the reverse curve of the hysteresis loop due to the contribution of the magnetic field trapped inside the grains. We have identified this remanent magnetic field at the GB by means of magneto-optical imaging.

Figure 13 shows the magnetic field distribution measured for a 0.2 μm YBCO thin film grown on a 4° [001] STO bicrystal in the remanent state. The magnetic field can be seen as black and white contrast (strong field in white) and the current distribution as contour lines, calculated from inversion of the Biot Savart's law.[29,42] The profiles of the critical current density and the magnetic field along the grain boundary are also shown. The figure clearly evidences the negative profile of magnetic field along the grain boundary. Note that although we have considered a constant average value of the magnetic field, there is certain inhomogeneity of the flux density as well as of the current density, typically observed for low-angle grain boundaries.[43]

B. Contribution of the grains far from a grain boundary to reverse magnetic field

The reverse component of the magnetic field at each grain boundary has been calculated by assuming that only two grains form a grain boundary contribute to the reverse field. Since the number of grains around a grain boundary increases proportionally to the distance, if there would be a notable contribution of the distant grains, the reverse field would depend on the sample dimension, i.e., on the number of grains around the grain boundary

We have patterned a disk in IBAD-b sample by standard photolithography, first with a radius $R_1 \sim 0.3$ cm and afterwards with $R_2 \sim 0.15$ cm. Figure 14 shows several magnetic hysteresis loops measured at 77 K at different maximum applied fields after each patterning. According to Eq. (9), the magnetic moment depends on the sample radius as $m = J_c \pi R^3 t/3$. Then, assuming that J_c^{GB} does not change after the patterning, the reduction of the magnetic moment will be given by

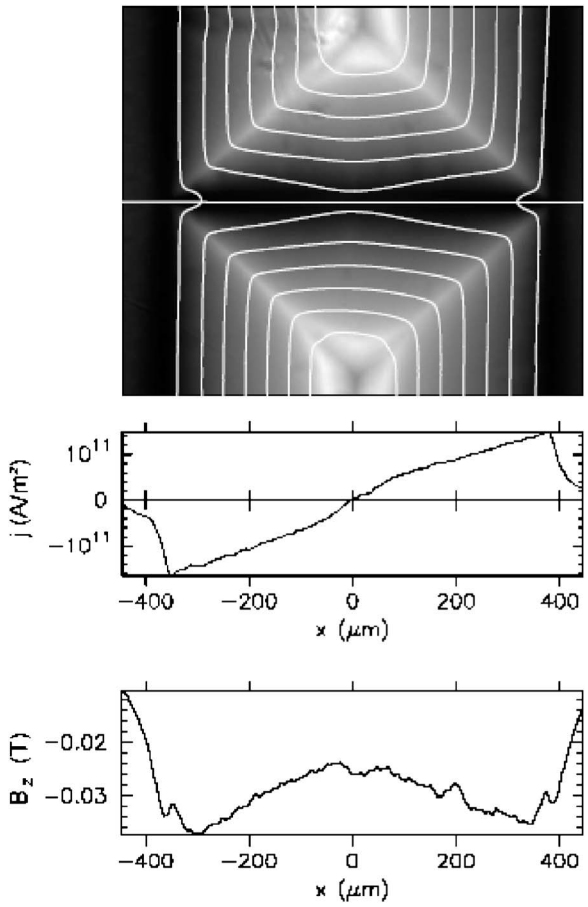

FIG. 13. Magneto Optical picture obtained at $T=4.2$ K for a 0.2 μm YBCO film grown on a 4° bicrystal, in the remanent state, with the current distribution visible as contour lines. Also shown are the current and field profiles along the GB.

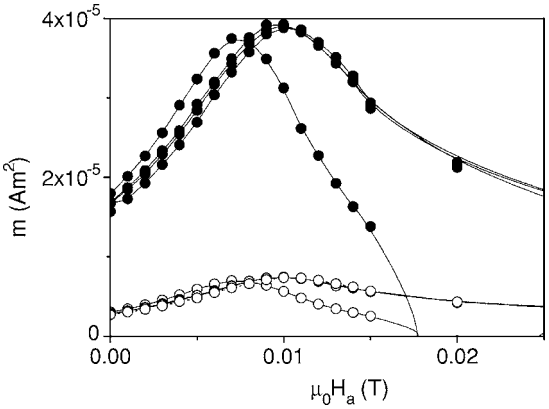

FIG. 14. Magnetic hysteresis loops measured for IBAD-b patterned as a disk of radius R_1 (closed symbols) and R_2 (open symbols) at 77 K and $\mu_0 H_m = 0.02$, 0.05, 0.1, and 0.2 T.

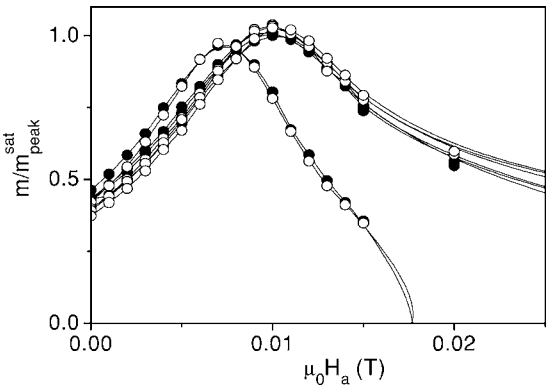

FIG. 15. Magnetic hysteresis loops normalized to m_{peak}^{sat}, measured at 77 K, for the sample IBAD-b patterned as a disk of radius R_1 (closed symbols) and R_2 (open symbols).

$$\frac{m_1}{m_2} = \frac{R_1^3}{R_2^3}. \tag{11}$$

We have determined an accurate value of the sample radius by using the initial slope of the first magnetization curve which is the magnetic susceptibility in case of perfect screening, χ_0, and can be calculated analytically for a thin disk in the Meissner state as[44]

$$\chi_0 = \frac{dM}{dH} = \frac{8R}{3\pi t}. \tag{12}$$

The values obtained for R_1=0.27 cm and R_2=0.15 cm agree with the experimental ones measured in optical images. With these values and using Eq. (11) one finds the ratio m_1/m_2=5.8, while from the experimental magnetic hysteresis loops we have m_1/m_2=5.3. The agreement between these two values confirms that the total magnetic moment measured is associated to the GB contribution (which depends on the sample radius) and no extra contribution from the grains is appreciated.

Although the patterning strongly affects the value of the magnetic moment in the hysteresis loop, the fact of having a sample with a smaller radius does not change the position of the peak and the saturation of the remanent magnetization. Figure 15 shows the hysteresis loops presented in Fig. 14 normalized to m_{sat}^{peak}, where the evolution of the peak is clearerly observed. The magnetization peak appears at exactly the same position for the hysteresis loops measured after each patterning, confirming that we can neglect the contribution of the distant grains in the reverse component of the field through each grain boundary. Shown in Fig. 16 is the evolution of the remanent magnetization as a function of the maximum applied field. Closed symbols correspond to M^{rem}/M_{rem}^{sat} for the sample with R_1 and open symbols for R_2. Note that both curves show the same dependence with the applied magnetic field and that the remanent magnetization saturates at the same value $H_m(M_{rem}^{sat})$. This result confirms that the saturation of the magnetization is due to the remanent field associated to the grains and not due to the GB percolative paths.

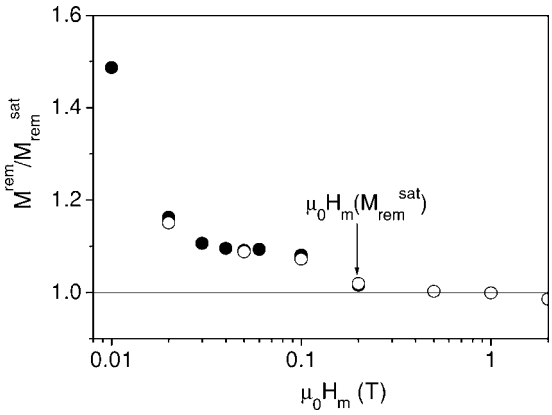

FIG. 16. Remanent magnetization, normalized to its saturated value, as a function of the maximum applied field for IBAD-b with R_1 (closed symbols) and with R_2 (open symbols). Also pointed is the maximum applied field that saturates M_{rem} in both cases.

C. Hysteretic behavior of J_c^{GB}

Granularity effects of flux trapping inside the grains have been previously observed by transport measurements in polycrystalline samples showing an hysteretic behavior of J_c^{GB}.[34] We have found the same $J_c^{GB}(H_a)$ hysteresis by means of inductive magnetic measurements, by applying Eq. (9) to both the initial and the reverse branches of the $M(H)$ curve. Figure 17 shows the $J_c^{GB}(H_a)$ values obtained for RABiTS-a at 77 K.

The hysteretic behavior observed can be attributed to granularity effects due to the different magnetic flux distribution appearing at the edge of the grains and contributing to the local field at the grain boundaries. By increasing the field, from ZFC, a positive magnetic field appears at the edge of each grain due to demagnetizing effects.[44] Therefore, the local field at the grain boundary can be determined by $H_{local}^{GB}=H_a+H_{edge}$ [Fig. 18(b)]. However, when decreasing the applied field in the reverse curve of the loop, the magnetic field appearing at the edge of the grains turns to be negative[44] and consequently $H_{local}^{GB}=H_a-H_{edge}$ [Fig. 18(a)]. Hence, the local field at the grain boundaries is different in the different branches of the loop, resulting in an asymmetric

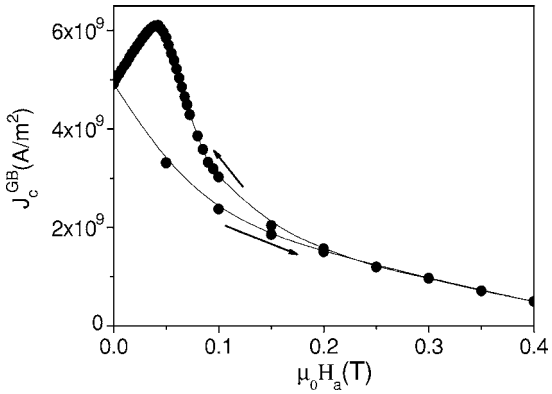

FIG. 17. $J_c^{GB}(H_a)$ dependence determined for RABiTS-a at 77 K and $\mu_0 H_m$=0.5 T. The hysteretic behavior of $J_c^{GB}(H_a)$ is clearly revealed.

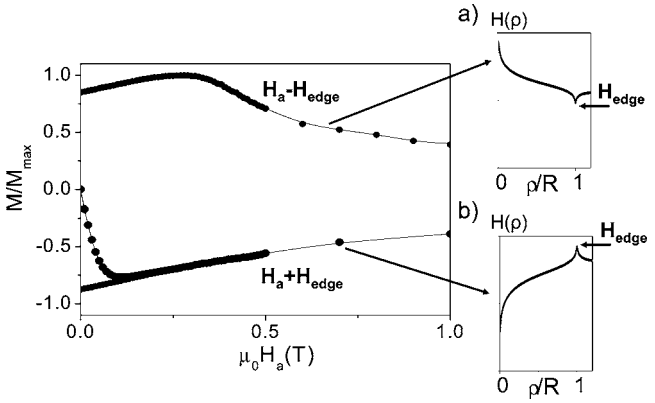

FIG. 18. Schematic representation of the local magnetic field at the grain boundaries determined at the different branches of the hysteresis loop. The magnetic field generated at the edge of a grain in the reverse curve of the loop, i.e., decreasing the applied field, is shown in (a) and increasing the field in (b).

hysteresis loop which gives an hysteretic behavior of $J_c^{GB}(H_a)$.

Additionally, the contribution of H_{edge} to the local magnetic field depends on the magnetic history of the grains. Figure 19 shows the first magnetization curve measured for an IBAD-coated conductor with $t=0.23$ μm and $\Delta\phi=7.8°$, IBAD-c, by increasing the magnetic field from ZFC (curve 1) and increasing the field after a complete saturated hysteresis loop (curve 2). The local magnetic field at the grain boundaries $H_{local}^{GB}=H_a+H_{edge}$, is lower in curve 1 than in curve 2, since the value of H_{edge} increases when the flux trapped inside the grains increases. Consequently, the two curves show an anomalous cross over.

D. Field cooled measurements

All the analysis of the hysteresis loops shown above, have been performed by measuring in ZFC condition, where the sample is cooled down from a temperature above T_c to the working temperature in zero applied magnetic field. Another possibility is to perform the measurement at field cool (FC) condition. In this case, a magnetic field H_m is applied at a

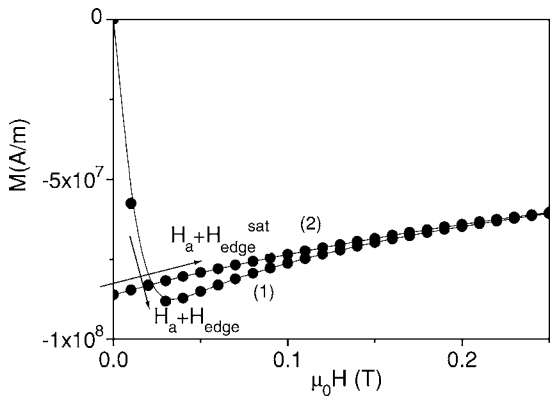

FIG. 19. Initial magnetization curve (1) and return curve after a complete saturated loop (2) measured for IBAD-c at 5 K and $\mu_0 H_m=0.5$ T.

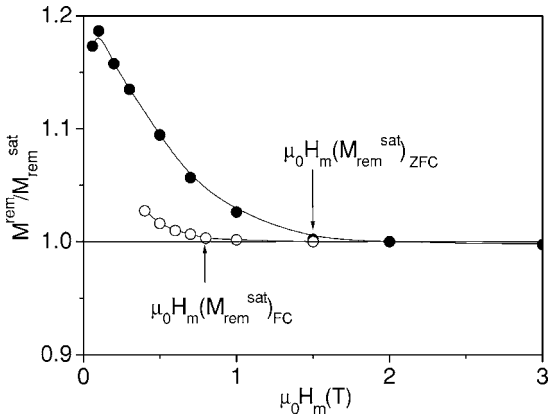

FIG. 20. M_{rem} normalized to M_{rem}^{sat} as a function of the maximum applied field H_m determined at ZFC (closed symbols) and FC (open symbols) for IBAD-c at 5 K.

temperature well above T_c and the sample is cooled down in the presence of this field. Then, the reverse magnetization from H_m down to zero can be measured.

According to the Bean critical state model, when a cylinder disk is cooled down in a ZFC process, the maximum applied field necessary to saturate the remanent magnetization is $H_m=2H^*$.[45] The same model determines that in FC condition, the remanent magnetization is already saturated for $H_m=H^*$.[45] Consequently, if the saturation of the remanent magnetization under ZFC condition occurs at $H_m(M_{rem}^{sat})=2H^*_G$, one expects that under FC conditions this saturation would occur at $H^*_G=H_m(M_{rem}^{sat})/2$. Figures 20 and 21 show the values of M_{rem}/M_{rem}^{sat} as a function of H_m determined at ZFC and FC, for IBAD-c at 5 K and for a RABiTS-a at 50 K, respectively. Note that, both confirm the condition $H_m(M_{rem}^{sat})_{FC}\sim(1/2)H_m(M_{rem}^{sat})_{ZFC}$, although the saturation of M_{rem} occurs in a different manner for each sample, i.e., for IBAD-c M_{rem} decreases until saturation while for RABiTS-a increases until saturation.

We have seen above that the saturation of M_{rem} occurs due to the saturation of the local magnetic field at the GB, i.e., saturation of the reverse field coming from the grains $H_{loc}^{sat}(H_a=0)\sim -H_{edge}^{max}(H_a=0)$. Then, M_{rem} should de-

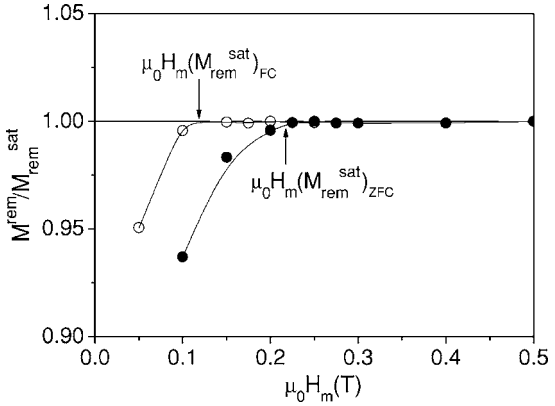

FIG. 21. M_{rem} normalized to M_{rem}^{sat} as a function of the maximum applied field H_m determined at ZFC (closed symbols) and FC (open symbols) for RABiTS-a at 50 K.

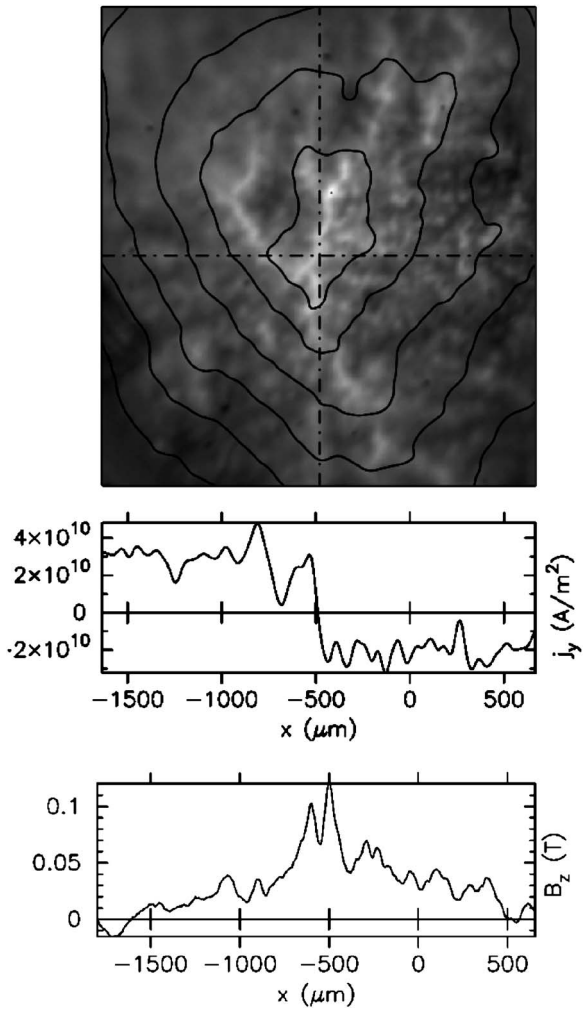

FIG. 22. Flux and current distribution of IBAD-d at 5 K, after FC the sample at $\mu_0 H_a = 260$ mT and reducing the magnetic field until $\mu_0 H_a = 39.6$ mT. External field have been subtracted and only self field is shown. Also presented are the current and magnetic flux profile at the position of the transversal line.

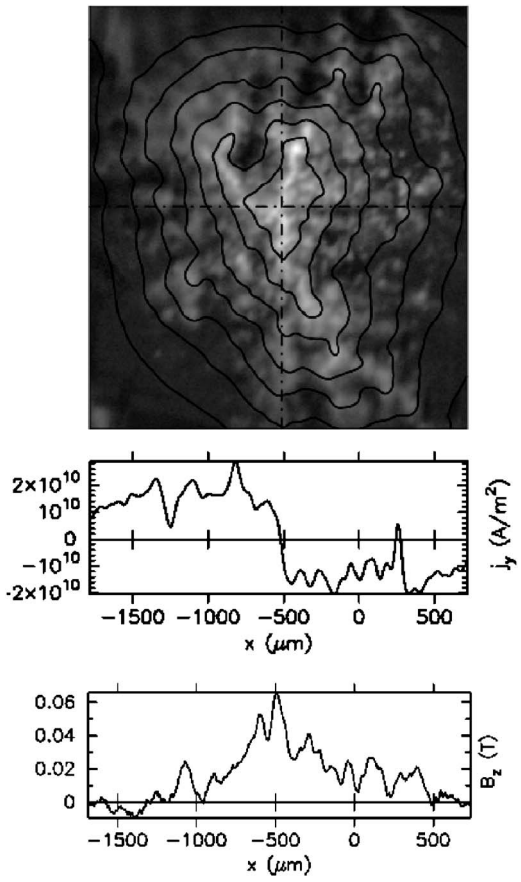

FIG. 23. Flux and current distribution of IBAD-d at 5 K, after FC the sample at $\mu_0 H_a = 260$ mT and reducing the magnetic field until $\mu_0 H_a = 0$ T. Also shown is the current and magnetic flux profile at the position of the transversal line.

crease when increasing H_m until it saturates, as it is observed in Fig. 20. However, for some of the coated conductors analyzed, the saturation of M_{rem} comes out increasing the value of M_{rem} until $M_{\mathrm{rem}}^{\mathrm{sat}}$ instead of decreasing it (Fig. 21). Although we do not have a clear explanation for this behavior, preliminary simulation of coated conductor hysteresis loops[40] shows that it could happen when not all the grains inside the sample saturate at the same magnetic field. This condition could be accomplished by assuming that the contribution of the self-magnetic field arising from the percolating GB critical currents is not negligible when the sample is still not saturated. It is important to remind that all the analysis to determine J_c^{GB} and J_c^{GB} is performed when the samples are already saturated, in which situation the self-field is negligible.[35,36]

E. Magneto-optical measurements

Granularity effects in the reverse magnetization curve of coated conductors have also been identified by magneto optical imaging. We have measured the magnetic flux distribution in an IBAD-coated conductor with $t = 1.6$ μm and $\Delta\phi = 12.7°$, IBAD-d, after field cooling the sample at $\mu_0 H_a = 260$ mT, and reducing the magnetic field following the return curve of the hysteresis loop. Figures 22 and 23 show the magnetic flux distribution as black and white contrast (strong field in white) obtained at 5 K, after decreasing the applied field down to $\mu_0 H_a = 39.6$ mT and $\mu_0 H_a = 0$ (remanent state), respectively. Pictures show the stray field of almost the complete sample. Irregular shape at some areas is due to bending nearby the sample edges. Contour lines represent the current distribution calculated from inversion of the Biot Savart's law.[29,42] Also the profiles of the critical current density and the magnetic field along the transversal line pointed in the pictures are shown. Grain size cannot be directly observed in the patterns since they are overview images taken below the highest resolution of the MO method.

For a nongranular film, due to the field dependence of J_c, one would obtain a higher trapped field at $\mu_0 H_a = 0$ T than at $\mu_0 H_a = 39.6$ mT but we observe that this is not the case for a coated conductor. At $\mu_0 H_a = 0$ mT the maximum trapped field in the centre of the sample is, $B_z \sim 0.06$ T while at $\mu_0 H_a = 39.6$ mT we get a higher value $B_z \sim 0.1$ T. This behavior can be understood considering that the local magnetic field at the grain boundaries have the contribution of the

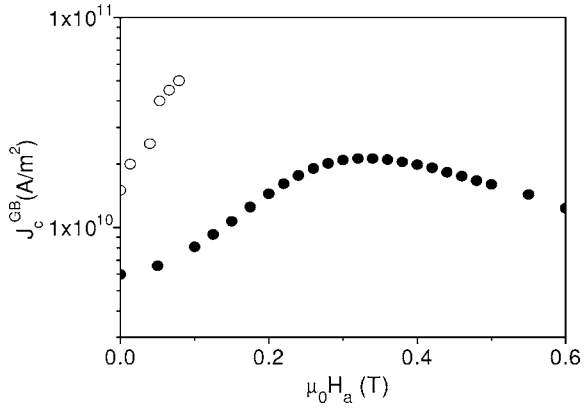

FIG. 24. GB critical current density as a function of the applied magnetic field, determined for IBAD-d at 5 K from MO measurements (open symbols) and from the saturate reverse branch of the hysteresis loop (closed symbols).

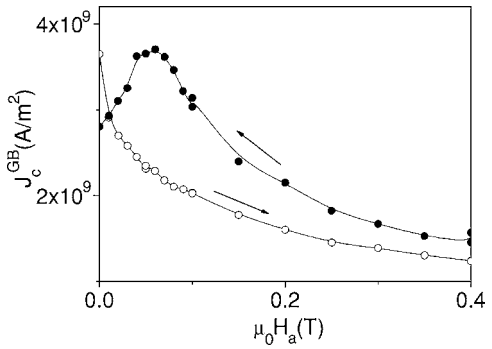

FIG. 25. Magnetic field dependence the transport critical current density measured for the sample IBAD-e at 25 K, by increasing (open symbols) and decreasing (closed symbols) the magnetic field until $\mu_0 H_m = 9$ T, where the hysteretic behavior of J_c is also revealed.

reverse component of the magnetic field coming from the grains, i.e., $H_{\mathrm{loc}}^{\mathrm{GB}} = H_a - H_{\mathrm{edge}}$. Then, as we have observed in the magnetic hysteresis loops, the local magnetic field at $\mu_0 H_a = 0$ mT is higher than that at $\mu_0 H_a = 39.6$ mT.

Due to GB inhomogeneities the critical current profiles are very irregular. Nevertheless, we clearly observe that the average value of critical current density obtained for the remanent state $J_c^{\mathrm{GB}} \sim 1.5 \times 10^{10}$ A/m^2 (Fig. 23) is smaller than the one obtained at $\mu_0 H_a = 39.6$ mT, $J_c^{\mathrm{GB}} \sim 2.5 \times 10^{10}$ A/m^2 (Fig. 22). We have measured the average J_c^{GB} at different applied fields describing the return branch of the hysteresis loop. Figure 24 shows the values of J_c^{GB} as a function of the applied magnetic field, determined from the MO images (open symbols) and from the saturated reverse branch of the magnetic hysteresis loop (closed symbols). Both curves show the same trend although there is a shift between them. The J_c difference could be associated to a systematic error in the measurement height of the stray field in MO which strongly influences the J_c values though not the tendency shown in Fig. 24. J_c^{GB} values from MO measurements could not be determined for applied magnetic fields above 0.1 T since the calibration of the magnetic flux at large magnetic field was not feasible.

F. Transport measurements

The hysteretic behavior of the percolative critical current density due to granularity effects has also been evidenced by means of transport measurements. Figure 25 shows the field dependence of the transport critical current density measured for an IBAD sample with $t = 1.2$ μm and $\Delta\phi = 6.5°$, IBAD-e, at 25 K increasing the applied field until $\mu_0 H_m = 9$ T and then decreasing it to zero. The similarity between the dependence $J_c(H_a)$ obtained by transport measurements and the data determined by means of the magnetic hysteresis loops (Fig. 17) is evident, confirming the experimental richness of the phenomena.

VI. CONCLUSION

We have analyzed the magnetic behavior of YBCO-coated conductors by means of dc-magnetization measurements of hysteresis loops. We have identified a shift in the peak position of the magnetization which has been ascribed to granularity effects and explained by means of the magnetic flux trapped inside the grains which have a reverse component through the grain boundaries. Based on the peculiar features observed in the coated conductor hysteresis loops and measuring several minor loops at different maximum applied fields, we have developed a formalism by which the grain and grain-boundary critical current densities J_c^{G} and J_c^{GB}, of coated conductors can be determined in the framework of the critical state model. The simplicity of the method paves the way to a full investigation of the relationship existing between these two critical current densities. We have checked the consistency of the formalism by doing additional magnetic measurements, as well as transport measurements and magneto-optical imaging. Systematic analysis using this methodology have been carried out enabling us to study important issues in coated conductors[24–26] with a much simpler methodology than transport measurements which require complex patterning of local grains and grain boundaries.

ACKNOWLEDGMENTS

This work has been supported by CICYT and FEDER (EU) (Grant Nos. MAT2002-02642, MAT2005-02047), Generalitat de Catalunya (Grant Nos. SGR2001-00189, 2005SGR-00029), CeRMAE, EU (SOLSULET Grant No. G5RD-CT2001-00550 and HIPERCHEM Grant No. NMP4-CT2005-516858). A.P. wishes to acknowledge MEC for financial support, SCENET for an exchange visit grant, and Generalitat de Catalunya for a Beatriu de Pinos contract. We would like to thank R. Feenstra and H.C. Freyhardt for samples supply and J. Gutierrez for performing transport measurements. Fruitful discussions and computer simulations with A. Sanchez and E. Pardo are gratefully acknowledged.

*Present address: Department of Materials Science, University of Cambridge, Pembroke Street, Cambridge CB2 3QZ, U.K.

[1] S. R. Foltyn *et al.*, IEEE Trans. Appl. Supercond. **9**, 1519 (1999).
[2] D. P. Norton *et al.*, Science **274**, 755 (1996).
[3] L. Civale *et al.*, J. Low Temp. Phys. **135**, 87 (2004).
[4] S. R. Foltyn *et al.*, Appl. Phys. Lett. **82**, 4519 (2003).
[5] D. Dimos, P. Chaudhari, J. Mannhart, and F. K. LeGoues, Phys. Rev. Lett. **61**, 219 (1988).
[6] H. Hilgenkamp and J. Mannhart, Rev. Mod. Phys. **74**, 485 (2002).
[7] D. M. Feldmann *et al.*, Appl. Phys. Lett. **77**, 2906 (2000).
[8] L. Fernandez *et al.*, Phys. Rev. B **67**, 052503 (2003).
[9] D. T. Verebelyi *et al.*, Appl. Phys. Lett. **76**, 1755 (2000).
[10] J. E. Evetts *et al.*, Semicond. Sci. Technol. **12**, 1050 (1999).
[11] B. Holzapfel *et al.*, IEEE Trans. Appl. Supercond. **11**, 3872 (2001).
[12] N. A. Rutter, B. A. Glowacki, and J. E. Evetts, Semicond. Sci. Technol. **13**, L25 (2000).
[13] E. D. Specht, A. Goyal, and D. M. Kroeger, Semicond. Sci. Technol. **13**, 592 (2000).
[14] A. Gurevich *et al.*, Phys. Rev. Lett. **88**, 097001 (2002).
[15] J. Albrecht, S. Leonhardt, and H. Kronmuller, Phys. Rev. B **63**, 014507 (2000).
[16] A. Gurevich and L. D. Cooley, Phys. Rev. B **50**, 13563 (1994).
[17] C. Jooss and J. Albrecht, Z. Metallkd. **93**, 1065 (2002).
[18] A. Palau *et al.*, Phys. Rev. B **73**, 132508 (2006).
[19] M. A. Angadi *et al.*, Physica C **185**, 1931 (1991).
[20] K. H. Muller, C. Andrikidis, H. K. Liu, and S. X. Dou, Phys. Rev. B **50**, 10218 (1994).
[21] S. Tonies, A. Vostner, and H. W. Weber, J. Appl. Phys. **92**, 2628 (2002).
[22] D. M. Feldmann *et al.*, Appl. Phys. Lett. **79**, 3998 (2001).
[23] A. Palau *et al.*, Appl. Phys. Lett. **84**, 230 (2004).
[24] A. Palau *et al.*, IEEE Trans. Appl. Supercond. **15**, 2790 (2005).
[25] A. Palau *et al.*, Appl. Phys. Lett. **88**, 122502 (2006).
[26] A. Palau *et al.*, Appl. Phys. Lett. **88**, 132508 (2006).
[27] A. Usoskin *et al.*, IEEE Trans. Appl. Supercond. **11**, 3385 (2001).
[28] R. Feenstra *et al.*, IEEE Trans. Appl. Supercond. **15**, 2803 (2005).
[29] C. Jooss *et al.*, Rep. Prog. Phys. **65**, 651 (2002).
[30] A. Sanchez and C. Navau, Phys. Rev. B **64**, 214506 (2001).
[31] K. H. Muller, C. Andrikidis, and Y. C. Guo, Phys. Rev. B **55**, 630 (1997).
[32] D. V. Shantsev *et al.*, Phys. Rev. Lett. **82**, 2947 (1999).
[33] J. R. Thompson *et al.*, Phys. Rev. B **69**, 104509 (2004).
[34] J. E. Evetts and B. A. Glowacki, Cryogenics **28**, 641 (1988).
[35] A. Sanchez and C. Navau, Semicond. Sci. Technol. **14**, 444 (2001).
[36] D. V. Shantsev, Y. M. Galperin, and T. H. Johansen, Phys. Rev. B **61**, 9699 (2000).
[37] M. Daumling and D. C. Larbalestier, Phys. Rev. B **40**, 9350 (1989).
[38] Th. Schuster, H. Kuhn, and E. H. Brandt, Phys. Rev. B **54**, 3514 (1996).
[39] A. O. Ijaduola *et al.*, Phys. Rev. B **73**, 134502 (2006).
[40] A. Palau, Ph.D. thesis, http://www.tdx.cesca.es/TDX-1201105-143027/, 2005
[41] D. Larbalestier, A. Gurevich, D. M. Feldmann, and A. Polyanskii, Nature (London) **414**, 368 (2001).
[42] C. Jooss, R. Warthmann, A. Forkl, and H. Kronmuller, Physica C **299**, 215 (1998).
[43] K. Guth, V. Born, and C. Jooss, Eur. Phys. J. B **42**, 239 (2004).
[44] J. R. Clem and A. Sanchez, Phys. Rev. B **50**, 9355 (1994).
[45] C. P. Bean, Phys. Rev. Lett. **8**, 250 (1962).